symmetry

MDPI

Article

Blind RIS Aided Ordered NOMA: Design, Probability of Outage Analysis and Transmit Power Optimization

Hindavi Kishor Jadhav and Vinoth Babu Kumaravelu *

Department of Communication Engineering, School of Electronics Engineering, Vellore Institute of Technology, Vellore 632014, Tamil Nadu, India
* Correspondence: vinothbab@gmail.com

Abstract: Non-orthogonal multiple access (NOMA) has been widely acclaimed as a promising solution to enhance spectral efficiency, increase user fairness, and scale up the number of users in wireless networks by enabling multiple users to share the symmetrical wireless resources. This work is concerned with the development and implementation of blind reconfigurable intelligent surface (RIS)-aided ordered NOMA (ONOMA) for smart reflector (SR) and access point (AP) configurations. For the RIS-SR-ONOMA and RIS-AP-ONOMA configurations, the closed-form probability of outage expressions is derived, and their performance is reported for distinct values of passive reflector elements. Through optimal power allocation, the downlink (DL) sum capacity is maximized. RIS-aided ONOMA reduces outage rates and increases sum capacity over the traditional ONOMA system. It is discovered that the RIS-aided ONOMA system increases the sum capacity by ≈33% at 20 dB signal-to-noise ratio (SNR) for 32 passive reflector elements. The addition of passive reflector elements and symmetrical allocation among users improves the performance of RIS-SR-ONOMA and RIS-AP-ONOMA in terms of outage probability, sum capacity, and probability of error. The proposed work can be employed in applications such as vehicular ad hoc networks, where obtaining precise channel information is difficult due to the rapid mobility of the vehicles.

Keywords: access point (AP); ordered non-orthogonal multiple access (ONOMA); probability of outage; reconfigurable intelligent surfaces (RIS); smart reflectors (SR); sum capacity; transmit power optimization

Citation: Jadhav, H.K.; Kumaravelu, V.B. Blind RIS Aided Ordered NOMA: Design, Probability of Outage Analysis and Transmit Power Optimization. *Symmetry* **2022**, *14*, 2266. https://doi.org/10.3390/sym14112266

Academic Editors: Mihai Postolache, Jia Hou, Jun Li and Xueqin Jiang

Received: 15 September 2022
Accepted: 22 October 2022
Published: 28 October 2022

1. Introduction

During the COVID-19 epidemic, people have become increasingly reliant on digital services like online shopping, food delivery, digital payments, education, and video streaming. In contrast to fifth-generation (5G) systems, sixth-generation (6G) systems are expected to meet high-performance requirements: spectrum efficiency increases to 100 b/s/Hz; connections are number of times higher (10^7 devices per km^2), and low latency (0.1 ms) [1–3]. Increasing user connections in 6G wireless systems can be accomplished with the non-orthogonal multiple access (NOMA) technique [4,5]. The evolution of wireless communication systems, an overview of 6G enabling technologies, new applications and various open research challenges related to 6G are briefly discussed in [6].

The base station (BS) of a downlink (DL) NOMA system allocates different power factors to multiple users who share the symmetrical orthogonal resources (i.e., space, time, frequency, codes) [7]. NOMA can be divided into two groups: Fixed NOMA (FNOMA) and Ordered NOMA (ONOMA). User decoding order in FNOMA is fixed, whereas it is based on channel gains in ONOMA. While the weak user (*WU*) with the lower channel gain is decoded first in ONOMA, the distant user is decoded first in FNOMA [8]. The receiver in NOMA uses the successive interference cancellation (SIC) approach to decode the superposed information.

To improve the quality of service (QoS) of wireless environment, there has been a surge in interest in managing the propagation environment. With the aid of reconfigurable antennas or scatterers, schemes like spatial scattering modulation [9], and beam index modulation [10], take advantage of the variations in the signatures of received signals to transmit extra information bits in environments with a lot of scattering. On the other hand, reflector arrays, meta-surfaces and substantial intelligent surface are intelligent tools that manage the propagation environment in order to increase coverage and quality of signal [11]. In contrast to multiple-input-multiple-output (MIMO), amplify-and-forward relaying, and backscatter communication, the reconfigurable intelligent surface (RIS) only reflects the incident signal with a phase shift and does not require separate energy source for processing, encoding, decoding, or retransmission [12]. RIS technology is intended to be utilized in addition to algorithms to build the hardware framework for artificial intelligence (AI) in the next-generation of wireless networks [13]. Table 1 provides a list of symbols used in this work.

Table 1. List of symbols.

Symbol	Description
u_i	Channel between BS and RIS
v_i	Channel between RIS and user equipment (UE)
α_i	Power allocation factor assigned to user i
x_s	Combined transmited signal
y_i	The received signal at user i
n_i	Complex Gaussian noise added at user i
L	Overall gain of the channel of user 1
M	Overall gain of the channel of user 2
$P_i^{o_{SR}}$	Probability of outage of user i for smart reflector (SR) scenario
P_i^{FNOMA}	Probability of outage of user i for FNOMA system
P_i^{ONOMA}	Probability of outage of user i for ONOMA system
$\dot{\mathrm{D}}_i$	Desired rate of user i
α_i^{subopt}	Sub-optimal power allocated to user i
α_i^{opt}	Optimal power allocated to user i

The remainder of this paper is organized as follows: Section 2 conducts a literature study, and Section 3 derives the closed-form outage probability and optimal power fractions for stronger user (SU) and WU. The performance of the proposed schemes is evaluated in Section 4 in terms of probability of outage, sum capacity, throughput, and probability of error. Finally, Section 5 concludes the work and offers directions for future research.

2. Literature Review

Intelligent surfaces that can be reconfigured are also envisaged as the massive MIMO 2.0 solution in 6G and are being studied in [14]. In [14], a comprehensive overview of the key enablers for the future generation of wireless networks, a description of their essential uses, and an overview of the existing and future research and development of these technologies is provided. An approach for configuring and standardizing next-generation wireless systems based on transmission through RIS that intentionally change the phases of incident waves is presented in [11]. Dual-hop (DH) and access point (AP)-based RIS configurations are presented and implemented in [11], where the findings prove that RIS can improve the symbol error rate performance especially at low signal-to-noise ratio (SNR) regions. In [15], blindness compensation is investigated using RIS for millimeter wave wireless networks. An algorithm based on stochastic gradient descent was proposed in this work for locating and orienting single and multi-RIS systems optimally. A real-time RIS prototype with 160 elements for sub-6 GHz is implemented and its performance is evaluated in [16]. Future directions to improve the performance of beamforming are also listed in [16]. A review of recent developments in RIS hardware systems, real-time considerations, and modeling of RIS systems is provided in [17]. In [18], an analytical study is conducted on a multiple-user MIMO wireless communication system that utilizes a RIS. A joint coherent/non coherent scheme is also explored in this study, examining the trade-off between performance and complexity. The article [7] focused on the evolution of NOMA and how it will meet the overgrowing requirements of next-generation wireless networks. An examination of the theoretic capacity bounds of NOMA, additional requirements and potential candidates for next-generation multiple access are presented. After evaluating the most recent research contributions on NOMA, the authors analyzed the potential of the technology, how it interacts with other new physical layering approaches, and the effect of utilizing multi-antenna system at DL or uplink (UL) [7].

There are several topics discussed in [19], including fundamentals of NOMA, the effects of incorporating multiple antennas at UL and DL, comparisons between orthogonal multiple access (OMA) and NOMA techniques, and NOMA categories such as power domain and code domain. It also discusses distinct resource sharing methodologies and power allocation strategies for NOMA. The concept of MIMO-NOMA and its limitations and directions for future research in this area by integrating NOMA with massive/millimeter wave MIMO are discussed in [20].

In [21], NOMA is integrated with RIS to improve bit error rate (BER) performance over conventional NOMA systems. A DL RIS-NOMA system is implemented in [22]. RIS-NOMA performs better than traditional NOMA is demonstrated in this work. In this study, it is shown that RISs can change user channel gains, therefore the SIC order in NOMA systems can be changed. A three-node cooperative relaying (CRS) system based on spatial modulation (SM)-aided NOMA (CRS-SM-NOMA) system is proposed in [23], where messages for two users are transmitted by two different information-bearing units of SM. In [24], RIS-based two user DL NOMA system is implemented for delay sensitive scenario and its effective capacity is estimated. Combining code-domain NOMA and RIS to implement massive MIMO in a clustered deployment is examined in [25]. By using code-domain NOMA, cluster-wide multi-user transmission is supported. The physical layer security of RIS-aided NOMA system is investigated in [26]. Moreover, a scheme for optimally allocating the power for jamming and transmitting signals is proposed. The following research gaps are identified in the existing literature:

- The majority of the classic works examined the FNOMA system.
- ONOMA, which is anticipated to outperform FNOMA in terms of outage performance for SU, has received very little research attention.
- In the majority of works, intelligent transmission schemes are taken into consideration, and it is believed that RIS has perfect channel knowledge for pre- and post-phase compensation. However, because of the increased mobility of vehicles, perfect channel knowledge may not be available in applications like vehicular ad hoc networks.
- As far as we are aware, there is no literature that has been proposed for the blind RIS-aided ONOMA system.
- The closed-form outage probability and sum capacity expressions for blind RIS-ONOMA are not found in any conventional literature.
- The computationally efficient strategy for optimizing the power fraction allocation to maximize the sum capacity is not discussed.
- The majority of classic study treats RIS as SR and deploys it in an environment far from the BS and receiver. Longer distances may result in weaker signals being received by RIS, which limits the array and diversity gain benefits. There are very few works that consider both SR and AP scenarios.

NOMA may not perform always better than OMA. When the channel gains of different users are same, the conventional OMA is the better option than NOMA. Hence in this work, we tried to incorporate RIS-assisted communication for NOMA to improve sum capacity, throughput, outage, and probability of error performances. In this work, we tried to show that even blind RIS without phase compensation improves sum capacity, throughput, outage, and probability of error performance. The significant contributions of this work are as follows:

- A novel blind-RIS-assisted ONOMA system model is proposed.
- The closed-form outage probability expressions have been derived for SR and AP scenarios of WU and SU.
- In order to maximize the DL sum capacity, the expressions for optimal power fraction allocation are derived.
- Probability of outage expressions for WU and SU are validated with Monte-Carlo simulations.

3. Outage Probability of RIS-ONOMA

In this section, the closed-form probability of outage expressions of RIS-ONOMA are derived for SR and AP configurations. In order to maximize the DL sum capacity, the optimal power fractions to allocate for *SU* and *WU* are also determined.

3.1. Probability of Outage of RIS-SR-ONOMA

Figure 1 depicts the block diagram of RIS-SR-ONOMA. It is assumed that user 1 is far from BS, whereas user 2 is nearer to BS. Here RIS consists of N passive reflecting elements that forms SR scenario, where symmetrical reflecting elements are assigned to *WU* and *SU* ($N_1 = N_2 = N/2$) irrespective of channel conditions. RIS is intended to generate any phase shift between 0 and 360 degrees. However, because of hardware limitations, it functions like an ON-OFF switch. It only generates a small number of discrete phase shifts. Therefore, in many real-world scenarios, the implementation of intelligent RIS assisted transmission is impractical. We cannot accomplish diversity gain in blind transmission since phase compensation is not performed at the RIS elements; instead, only array gain can be attained. BS and RIS communicate using one channel with a channel coefficient $u_i = a_i e^{j\Phi_i}$ and RIS and UE communicate via the other channel with a channel coefficient $v_i = b_i e^{j\psi_i}$. Both $u_i \in \mathbb{C}N(0,\ 1)$ and $v_i \in \mathbb{C}N(0,\ 1)$ follow Rayleigh distribution [27].

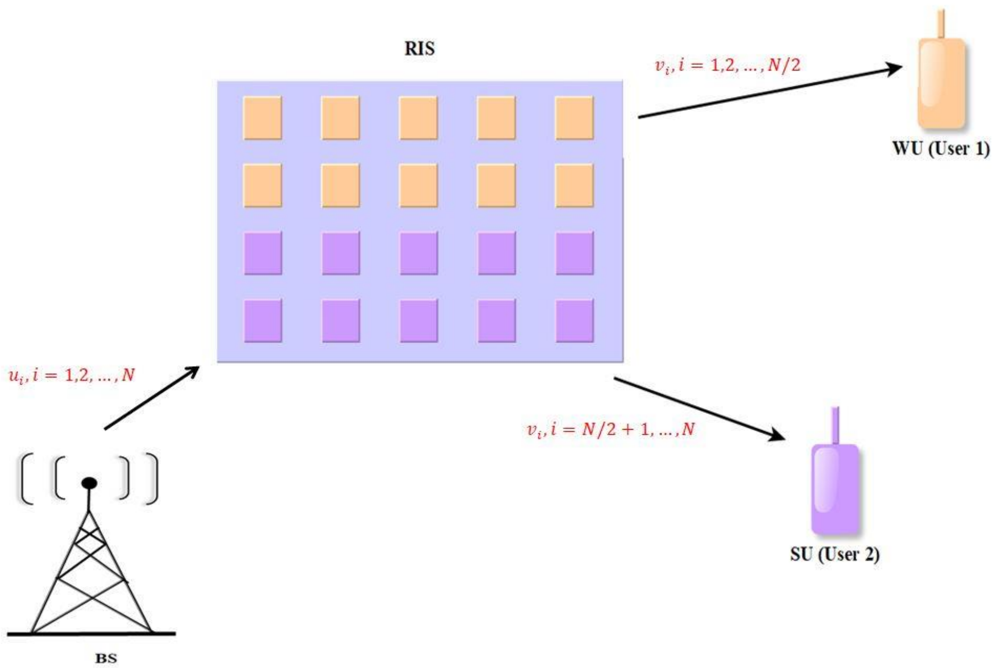

Figure 1. Pictorial representation of RIS-SR-ONOMA system.

To implement the NOMA coding principle, BS combines two independent signals using the superposition coding method, and then transmits this combined signal to the users which is given by [28]

$$x_s = \sqrt{\alpha_1 E_s} x_1 + \sqrt{\alpha_2 E_s} x_2 \tag{1}$$

Here α_1 and α_2 are the power allocation factors assigned to user 1 and 2 respectively. In ONOMA $\alpha_2 < \alpha_1$ and the sum of power allocation factors must be equal to unity which is given as

$$\alpha_1 + \alpha_2 = 1 \tag{2}$$

Intended symbols for user 1 and 2 are denoted by x_1 and x_2 respectively. E_s represents average transmit power of the symbols x_1 and x_2.

The received signal y_1 at user 1 is given by

$$y_1 = \left[\sum_{i=1}^{\frac{N}{2}} u_i v_i\right] x_s + n_1 \tag{3}$$

Here n_1 is the complex Gaussian noise added at user 1 with variance N_0. Let $L = \sum_{i=1}^{\frac{N}{2}} u_i v_i$ is the overall gain of the dual-hop channel. As per the central limit theorem (CLT), L follows complex Gaussian distribution $L \in \mathcal{CN}(0, N_1)$ [27]. After substituting (1) in (3), the received signal at user 1 is given as,

$$y_1 = L\sqrt{\alpha_1 E_s} x_1 + L\sqrt{\alpha_2 E_s} x_2 + n_1 \tag{4}$$

The user with the maximum power i.e., user 1 regards the signal from user 2 as interference and recovers its signal without going through any SIC process. The signal-to-interference plus noise ratio (SINR) of user 1 is

$$\Upsilon_1^{x_1} = \frac{|L|^2 \alpha_1 \varrho_s}{|L|^2 \alpha_2 \varrho_s + 1} \tag{5}$$

where $\varrho_s = \frac{E_s}{N_0}$ represents received SNR. The capacity of user 1 is given by

$$C_1^{x_1} = log_2\left(1 + \Upsilon_1^{x_1}\right) \tag{6}$$

Similarly, the received signal y_2 at user 2 is given as,

$$y_2 = \left[\sum_{i=\frac{N}{2}+1}^{N} u_i v_i\right] x_s + n_2 \tag{7}$$

Here n_2 is the complex Gaussian noise added at user 2 with variance N_0. Let $M = \sum_{i=\frac{N}{2}+1}^{N} u_i v_i$ is the overall gain of the two-hop channel. As per the CLT, M follows complex Gaussian distribution $M \in \mathcal{CN}(0, N_2)$ [27]. After substituting (1) in (7), the received signal at user 2 is given as,

$$y_2 = M\sqrt{\alpha_1 E_s} x_1 + M\sqrt{\alpha_2 E_s} x_2 + n_2 \tag{8}$$

At user 2, user 1's signal is detected first assuming user 2's signal as interference. The SINR of decoding user 1's signal at user 2 is given by

$$\Upsilon_2^{x_1} = \frac{|M|^2 \alpha_1 \varrho_s}{|M|^2 \alpha_2 \varrho_s + 1} \tag{9}$$

After the estimation process of x_1, its impact is removed from y_2 through SIC. The residual signal is given by

$$\widetilde{y}_2 = M\sqrt{\alpha_2 E_s} x_2 + n_2 \tag{10}$$

After SIC, the SNR of user 2 is given as

$$\Upsilon_2^{x_2} = |M|^2 \alpha_2 \varrho_s \tag{11}$$

The capacity of user 2 is given by

$$C_2^{x_2} = log_2\left(1 + \Upsilon_2^{x_2}\right) \tag{12}$$

The channel gains of user 1 $\left(\beta_1 = |L|^2\right)$ and 2 $\left(\beta_2 = |M|^2\right)$ follow Chi-square distribution with two degrees of freedom [29]. The probability density functions (PDF) of β_1 and β_2 are given by

$$f_{B_1}(\beta_1) = \frac{1}{\delta_1^2 N_1} exp\left(\frac{-\beta_1}{\delta_1^2 N_1}\right) \tag{13}$$

$$f_{B_2}(\beta_2) = \frac{1}{\delta_2^2 N_2} exp\left(\frac{-\beta_2}{\delta_2^2 N_2}\right) \tag{14}$$

where B_1 and B_2 are the random variables corresponding to β_1 and β_2 respectively. Here $\delta_1^2 N_1$ and $\delta_2^2 N_2$ represent average channel gains of user 1 and 2 respectively, whose harmonic mean is given by

$$\frac{1}{\delta_H^2} = \frac{1}{\delta_1^2 N_1} + \frac{1}{\delta_2^2 N_2} \tag{15}$$

The *WU* is identified using

$$\widetilde{\beta}_{WU} = min(\beta_1, \beta_2) \tag{16}$$

The PDF of *WU* is given by

$$f_{\widetilde{B}_{WU}}(\widetilde{\beta}_{WU}) = \frac{1}{\delta_H^2} exp\left(\frac{-\widetilde{\beta}_{WU}}{\delta_H^2}\right) \tag{17}$$

The detailed derivation of this PDF is highlighted in Appendix A.
The probability of outage for *WU* is

$$P_{WU}^{o_{SR}} = Pr\left(log_2\left(1 + \Upsilon_1^{x_1}\right) \leq \dot{D}_{WU}\right) \tag{18}$$

Here $\dot{D}_{WU}$ is the desired rate of *WU*.
Replacing $\Upsilon_1^{x_1}$ from (5) in (18)

$$P_{WU}^{o_{SR}} = Pr\left[log_2\left(1 + \frac{|L|^2 \alpha_1 \varrho_s}{|L|^2 \alpha_2 \varrho_s + 1}\right) \leq \dot{D}_{WU}\right] \tag{19}$$

Simplifying (19) for $\widetilde{\beta}_{WU}$ gives

$$P_{WU}^{o_{SR}} = Pr\left[\widetilde{\beta}_{WU} \leq \underbrace{\frac{D_{WU}}{(\alpha_1 - \alpha_2 D_{WU})\varrho_s}}_{y_{WU}}\right] \tag{20}$$

Here $D_{WU} = 2^{\dot{D}_{WU}} - 1$. (20) can be written as

$$P_{WU}^{o_{SR}} = \int_0^{y_{WU}} f_{\widetilde{B}_{WU}}\left(\widetilde{\beta}_{WU}\right) d\widetilde{\beta}_{WU} \tag{21}$$

Substituting (17) in (21)

$$P_{WU}^{o_{SR}} = \int_0^{y_{WU}} \frac{1}{\delta_H^2} exp\left(\frac{-\widetilde{\beta}_{WU}}{\delta_H^2}\right) d\widetilde{\beta}_{WU} \tag{22}$$

After simplification, the probability of outage for WU is given as

$$P_{WU}^{o_{SR}} = 1 - exp\left(-\frac{D_{WU}}{(\alpha_1 - \alpha_2 D_{WU})\varrho_s \delta_H^2}\right) \tag{23}$$

The SU is identified using

$$\widetilde{\beta}_{SU} = max(\beta_1, \beta_2) \tag{24}$$

The PDF of SU is given by

$$f_{\widetilde{B}_{SU}}\left(\widetilde{\beta}_{SU}\right) = \frac{1}{\delta_1^2 N_1} exp\left(\frac{-\widetilde{\beta}_{SU}}{\delta_1^2 N_1}\right) + \frac{1}{\delta_2^2 N_2} exp\left(\frac{-\widetilde{\beta}_{SU}}{\delta_2^2 N_2}\right) - \frac{1}{\delta_H^2} exp\left(\frac{-\widetilde{\beta}_{SU}}{\delta_H^2}\right) \tag{25}$$

The detailed derivation of this PDF is highlighted in Appendix B.
The decoding of user 1 fails at user 2 when

$$log_2\left(1 + \Upsilon_2^{x_1}\right) < \dot{D}_{WU} \tag{26}$$

The decoding of user 2 fails at user 2 when

$$log_2\left(1 + \Upsilon_2^{x_2}\right) < \dot{D}_{SU} \tag{27}$$

where $\dot{D}_{SU}$ is the desired rate of SU and $D_{SU} = 2^{\dot{D}_{SU}} - 1$. The condition under which SU cannot detect its own signal is obtained by substituting (9) and (11) in (26) and (27) and solving for $\widetilde{\beta}_{SU}$. It is represented by

$$\widetilde{\beta}_{SU} \leq \underbrace{max\left\{\frac{D_{WU}}{(\alpha_1 - \alpha_2 D_{WU})\varrho_s}, \frac{D_{SU}}{\alpha_2 \varrho_s}\right\}}_{y_{SU}} \tag{28}$$

The probability of outage for SU is represented by

$$P_{SU}^{o_{SR}} = Pr\left[\widetilde{\beta}_{SU} \leq max\left\{\frac{D_{WU}}{(\alpha_1 - \alpha_2 D_{WU})\varrho_s}, \frac{D_{SU}}{\alpha_2 \varrho_s}\right\}\right] \tag{29}$$

The probability of outage for SU is calculated as

$$P_{SU}^{o_{SR}} = \int_0^{y_{SU}} f_{\widetilde{B}_{SU}}\left(\widetilde{\beta}_{SU}\right) d\widetilde{\beta}_{SU} \tag{30}$$

Substituting (25) in (30)

$$P_{SU}^{o_{SR}} = \int_0^{y_{SU}} \left(\frac{1}{\delta_1^2 N_1} exp\left(\frac{-\widetilde{\beta}_{SU}}{\delta_1^2 N_1}\right) + \frac{1}{\delta_2^2 N_2} exp\left(\frac{-\widetilde{\beta}_{SU}}{\delta_2^2 N_2}\right) - \frac{1}{\delta_H^2} exp\left(\frac{-\widetilde{\beta}_{SU}}{\delta_H^2}\right)\right) d\widetilde{\beta}_{SU} \tag{31}$$

After simplification, the probability of outage of SU becomes

$$P_{SU}^{o_{SR}} = 1 - exp\left(\frac{-y_{SU}}{\delta_1^2 N_1}\right) - exp\left(\frac{-y_{SU}}{\delta_2^2 N_2}\right) + exp\left(\frac{-y_{SU}}{\delta_H^2}\right) \tag{32}$$

3.2. Probability of Outage of RIS-AP-ONOMA

Figure 2 illustrates the RIS-aided AP-ONOMA system. In AP configuration, RIS is located near to transmitter. N passive reflectors are placed nearer to AP, hence the fading effect between AP and RIS is less effective. This scenario represents one-hop communication.

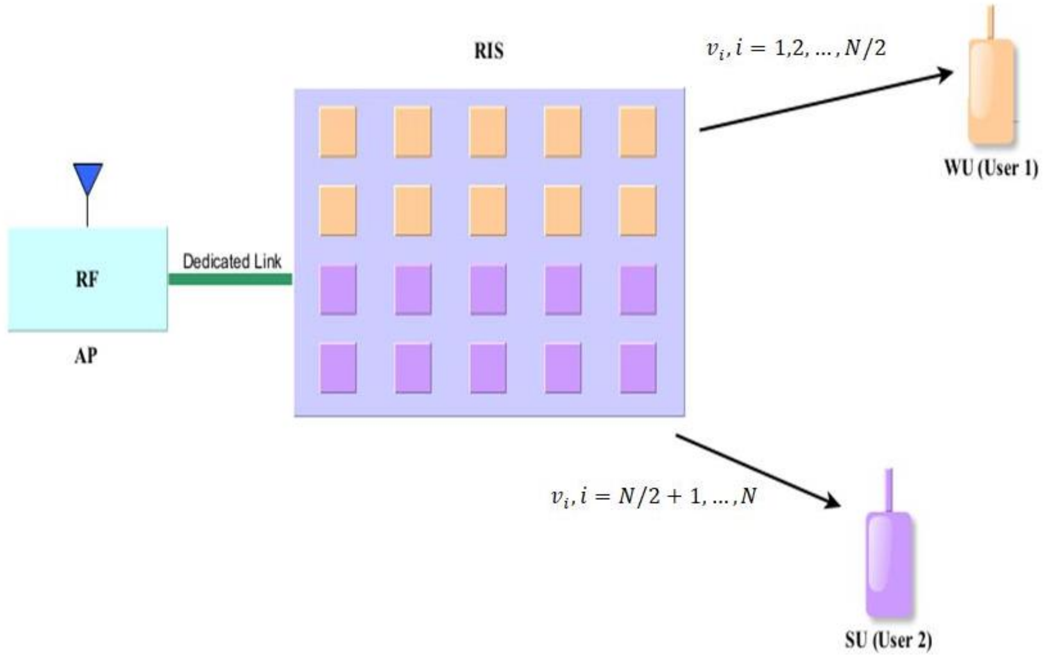

Figure 2. Pictorial representation of RIS-AP-ONOMA system.

The received signals y_1 at user 1 and y_2 at user 2 are given by

$$y_1 = \left[\sum_{i=1}^{\frac{N}{2}} v_i\right] x_s + n_1 \quad (33)$$

$$y_2 = \left[\sum_{i=\frac{N}{2}+1}^{N} v_i\right] x_s + n_2 \quad (34)$$

Let $P = \sum_{i=1}^{\frac{N}{2}} v_i$ and $Q = \sum_{i=\frac{N}{2}+1}^{N} v_i$ are the overall gains of the one-hop channel. As per the CLT, P and Q follow complex Gaussian distribution where $P \in \mathbb{C}\aleph(0, N_1)$ and $Q \in \mathbb{C}\aleph(0, N_2)$ [27].

Following the same procedure as in RIS-SR-NOMA, we can derive the PDF and probability of outage expressions for RIS-AP-NOMA.

3.3. DL Sum Capacity Maximization through Optimal Power Allocation

This section discusses in detail the optimal power fractions for RIS-SR-ONOMA and RIS-AP-ONOMA systems for maximizing DL sum capacity. The sum capacity of the RIS-SR-ONOMA system having two users at DL is given as

$$C_T = C_{SU} + C_{WU} = log_2\left(1 + \Upsilon_1^{x_1}\right) + log_2\left(1 + \Upsilon_2^{x_2}\right) \quad (35)$$

Here C_{SU} and C_{WU} represents capacities of SU and WU respectively. Both SU and WU power allocation factors α_2 and α_1 need to be optimized to maximize their sum capacity, while satisfying their QoS constraints listed in (2), (36) and (37)

$$log_2\left(1 + \Upsilon_1^{x_1}\right) \geq \dot{D}_{WU} \quad (36)$$

$$log_2\left(1 + \Upsilon_2^{x_2}\right) \geq \dot{D}_{SU} \quad (37)$$

Substituting (5) and (11) in (35) and simplifying,

$$C_T = log_2\left((1+\beta_1\varrho_s)\left(\frac{1+\beta_2\alpha_2\varrho_s}{1+\beta_1\alpha_2\varrho_s}\right)\right) \tag{38}$$

The term $(1+\beta_1\varrho_s)$ is constant. The sum capacity is increasing function of α_2, which lies in the interval:

$$\underbrace{\frac{D_{SU}}{\beta_2\varrho_s}}_{\alpha_2^{min}} \leq \alpha_2 \leq \underbrace{\frac{\beta_1\varrho_s - D_{WU}}{\beta_1\varrho_s(1+D_{WU})}}_{\alpha_2^{max}} \tag{39}$$

The condition in (39) is derived in detail in Appendix C.
α_2^{min} should be lower than α_2^{max}. Hence,

$$\frac{D_{SU}}{\beta_2\varrho_s} \leq \frac{\beta_1\varrho_s - D_{WU}}{\beta_1\varrho_s(1+D_{WU})} \tag{40}$$

To attain the QoS constraints, the overall SNR requirement of RIS-SR-ONOMA system is given by

$$\varrho_s \geq \frac{D_{SU}}{\beta_2} + \frac{D_{SU}D_{WU}}{\beta_2} + \frac{D_{WU}}{\beta_1} \tag{41}$$

The optimal value of α_2 is the largest value, which maximize the overall capacity. The optimal value of α_2 in RIS-SR-ONOMA is given by

$$\alpha_2^{opt} = \frac{\beta_1\varrho_s - D_{WU}}{\beta_1\varrho_s(1+D_{WU})} \tag{42}$$

The optimal value of α_1 in RIS-SR-ONOMA is given by

$$\alpha_1^{opt} = 1 - \alpha_2^{opt} \tag{43}$$

In the same fashion, we can obtain the optimal power fractions for RIS-AP-ONOMA system.

4. Simulation Results and Discussion

The results of Monte-Carlo simulations are provided in this section to verify the closed-form expressions derived in Section 3. All the parameters utilized in this analysis are listed in Table 2. The power fraction allocation, desired rates, average channel gains are selected based on [30,31]. Figure 3 compares the probability of outages for FNOMA, ONOMA, and RIS-SR-ONOMA for 32 passive reflector elements. The probability of outage expressions for *SU* and *WU* in FNOMA system are given by [28]

$$P_{WU}^{\text{FNOMA}} = 1 - exp\left(-\frac{D_{WU}}{(\alpha_1 - \alpha_2 D_{WU})\varrho_s\delta_1^2}\right) \tag{44}$$

$$P_{SU}^{\text{FNOMA}} = 1 - exp\left(\frac{-y_{SU}}{\varrho_s\delta_2^2}\right) \tag{45}$$

The probability of outage expressions for *SU* and *WU* in ONOMA system are given by [8,28]

$$P_{WU}^{\text{ONOMA}} = 1 - exp\left(-\frac{D_{WU}}{(\alpha_1 - \alpha_2 D_{WU})\varrho_s\delta_H^2}\right) \tag{46}$$

$$P_{SU}^{\text{ONOMA}} = 1 - exp\left(\frac{-y_{SU}}{\varrho_s\delta_1^2}\right) - exp\left(\frac{-y_{SU}}{\varrho_s\delta_2^2}\right) + exp\left(\frac{-y_{SU}}{\varrho_s\delta_H^2}\right) \tag{47}$$

At 5 dB SNR, the probabilities of outage are 0.3266, 0.3777, and 0.02921 for FNOMA-WU, ONOMA-WU and RIS-SR-ONOMA-WU respectively. Similarly, the probabilities of outage are 0.4697, 0.4488, and 0.0006951 for FNOMA-SU, ONOMA-SU and RIS-SR-ONOMA-SU respectively. It is observed that probability of outage performance of FNOMA is better for *WU*. ONOMA reduces the probability of outage of *SU* compared to FNOMA. A great improvement in outage probabilities can be seen when RIS is incorporated with ONOMA for *SU* and *WU*.

Table 2. Parameters used in this analysis [8,11,28,30–32].

Parameters	Value
Quantity of users	2
Quantity of reflecting elements	4,8,16,32,64,128,256,512
Average channel gain of *WU*	1
Average channel gain of *SU*	5
Target rate of *WU*	1 b/s/Hz
Target rate of *SU*	1 b/s/Hz
Target throughput	3 b/s/Hz
Power factor allocated to *WU*	0.1
Power factor allocated to *SU*	0.9
Block length	10^6 bits

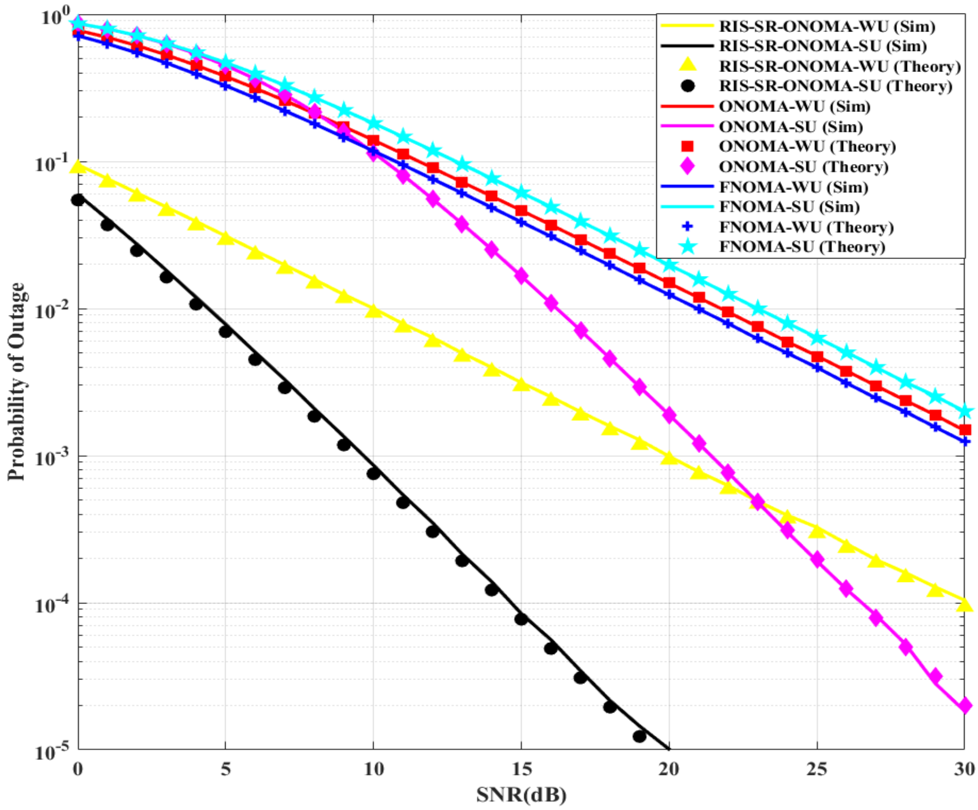

Figure 3. Comparison of probabilities of outage of *WU* and *SU* for FNOMA, ONOMA and blind RIS-SR-ONOMA.

Figure 4 depicts a probability of outage analysis for blind RIS-SR-ONOMA *SU* for various *N* values. It is observed that probability of outage performance of *SU* is better than *WU* for various *N*. A deviation in simulated and theoretical results is observed at lower values of *N*, such as 4, 8 and 16. As per (3) and (7), the principle of CLT is violated for lower values of *N*. After $N = 32$, the simulated and theoretical results became closely related, so the lower limit of $N = 32$ is fixed for the rest of the work. For $N = 32$, 64, 128, 256, and 512, the probabilities of outage are 0.006951, 0.001841, 0.0004741, 0.0001203 and 3.03×10^{-5}, at SNR of 5 dB respectively. According to (15), the increment in N increases δ_H^2. As per (32), a larger value of δ_H^2 decreases the $\left(\frac{-y_{SU}}{\delta_H^2}\right)$. The smaller value of negative exponential increases the $exp\left(\frac{-y_{SU}}{\delta_H^2}\right)$. As N increases $exp\left(\frac{-y_{SU}}{\delta_1^2 N_1}\right)$ and $exp\left(\frac{-y_{SU}}{\delta_2^2 N_2}\right)$ increases. As these two terms are more dominant in (32) than $exp\left(\frac{-y_{SU}}{\delta_H^2}\right)$, the probability of outage decreases for SU. This analysis is repeated for WU in Figure 5. The probabilities of outage are 0.02921, 0.01471, 0.007384, 0.003699 and 0.001851 for N = 32, 64, 128, 256, and 512 at SNR of 5 dB respectively. After substituting $N_1 = N_2 = N/2$ in (15), increment in N increases δ_H^2. As per (23), a larger value of δ_H^2 decreases the term $\left(-\frac{D_{WU}}{(\alpha_1-\alpha_2 D_{WU})\varrho_s \delta_H^2}\right)$. The smaller value of negative exponential increases the $exp\left(-\frac{D_{WU}}{(\alpha_1-\alpha_2 D_{WU})\varrho_s \delta_H^2}\right)$. This decreases the probability of outage for WU. As N increases, there is a decrease in outage probability and simulation and analytical results are almost identical. It is observed that probability of outage performance of SU is better than WU for various N.

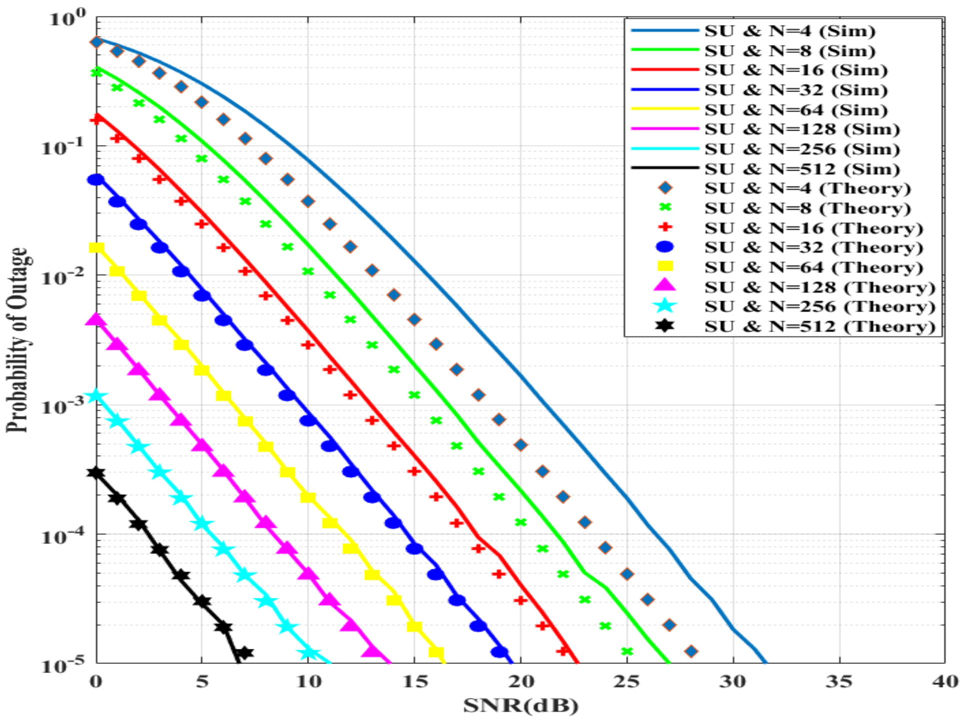

Figure 4. Probability of outage analysis of blind RIS-SR-ONOMA SU with distinct N.

In Figure 6, the outage performance of proposed system is analyzed for symmetric and asymmetric allocation of RIS elements to SU and WU. In symmetric scenario, equal number of RIS elements is allocated for SU and WU, whereas in asymmetric scenario, 75% of the elements are allocated to WU and remaining 25% of elements are allocated to SU. At SNR of 5 dB and for N = 512, the probability of outage of SU is 1.55×10^{-5} and 2.03×10^{-5} for symmetric and asymmetric scenarios respectively. Similarly, the probability of outage of WU is 0.0017 and 0.0014 for symmetric and asymmetric scenarios respectively. Due to the allocation of 75% of the elements to WU, the probability of an outage decreases in asymmetric scenario, whereas 25% of elements are allocated to SU, resulting in an increased probability of an outage of the asymmetric scenario.

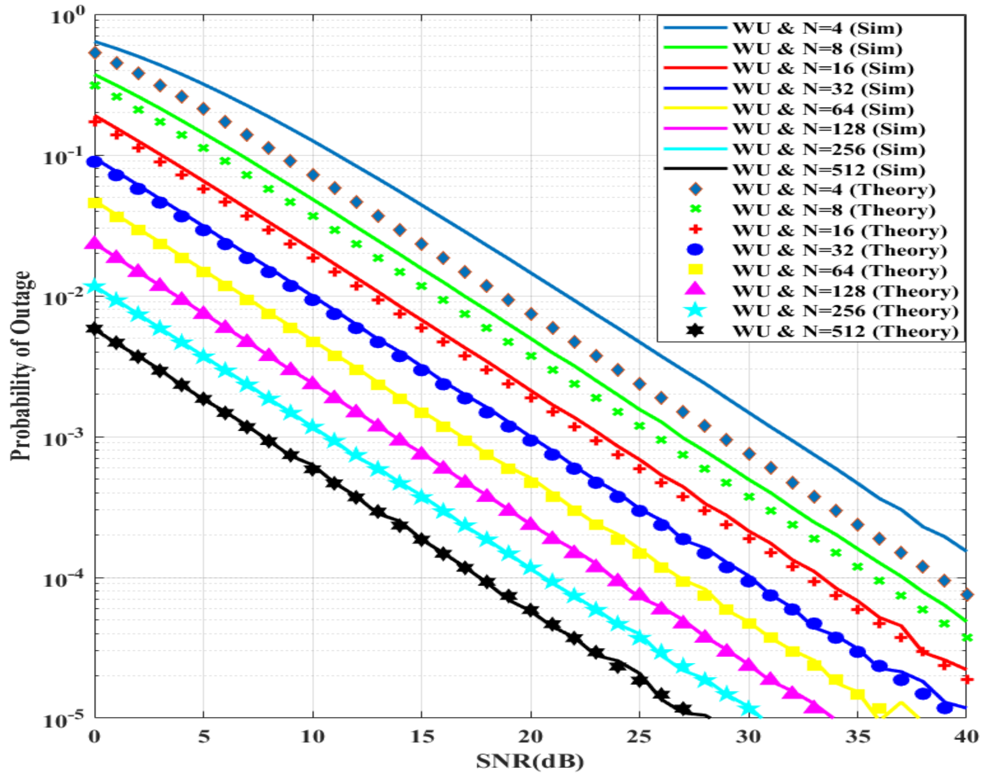

Figure 5. Probability of outage analysis of blind RIS-SR-ONOMA *WU* with distinct *N*.

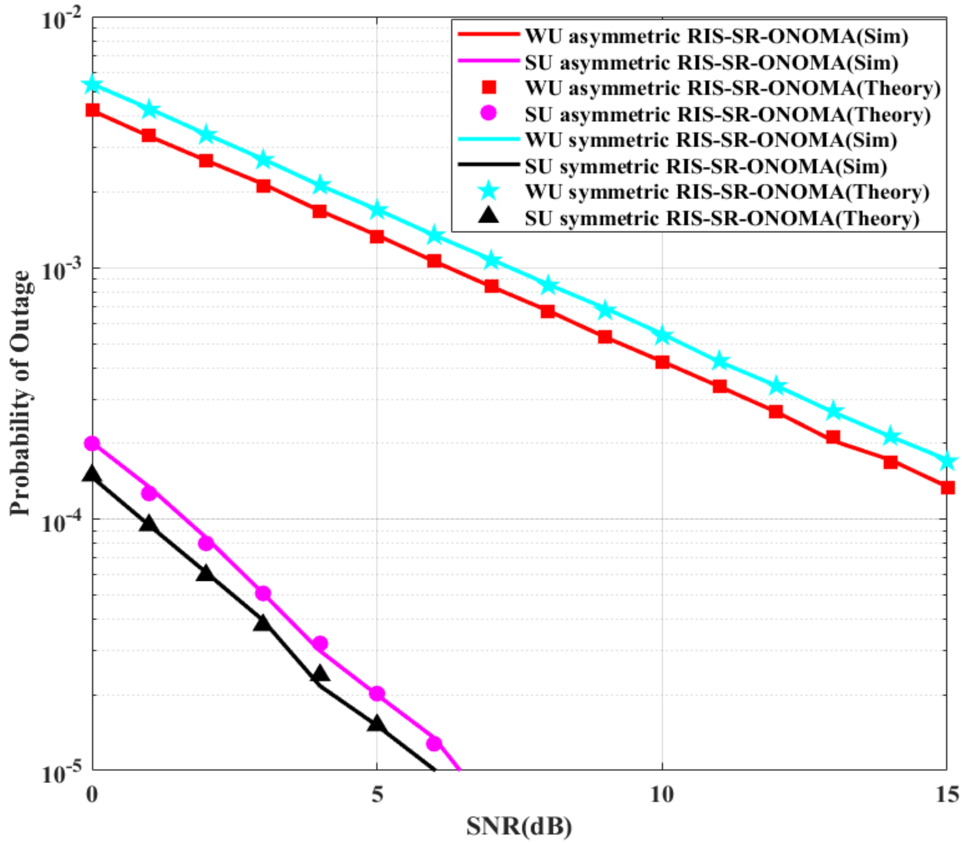

Figure 6. Probability of outage analysis of blind RIS-SR-ONOMA for symmetric and asymmetric scenarios.

The sum capacity analysis of blind RIS-SR-ONOMA for distinct values of N is carried out in Figure 7. The sum capacities (b/s/Hz) observed are 12.3883, 13.3942, 14.3978, 15.3936 and 16.3913 for N = 32, 64, 128, 256, and 512 respectively. In order to validate the performance of optimal power allocation, we used the following suboptimal power allocation for SU and WU:

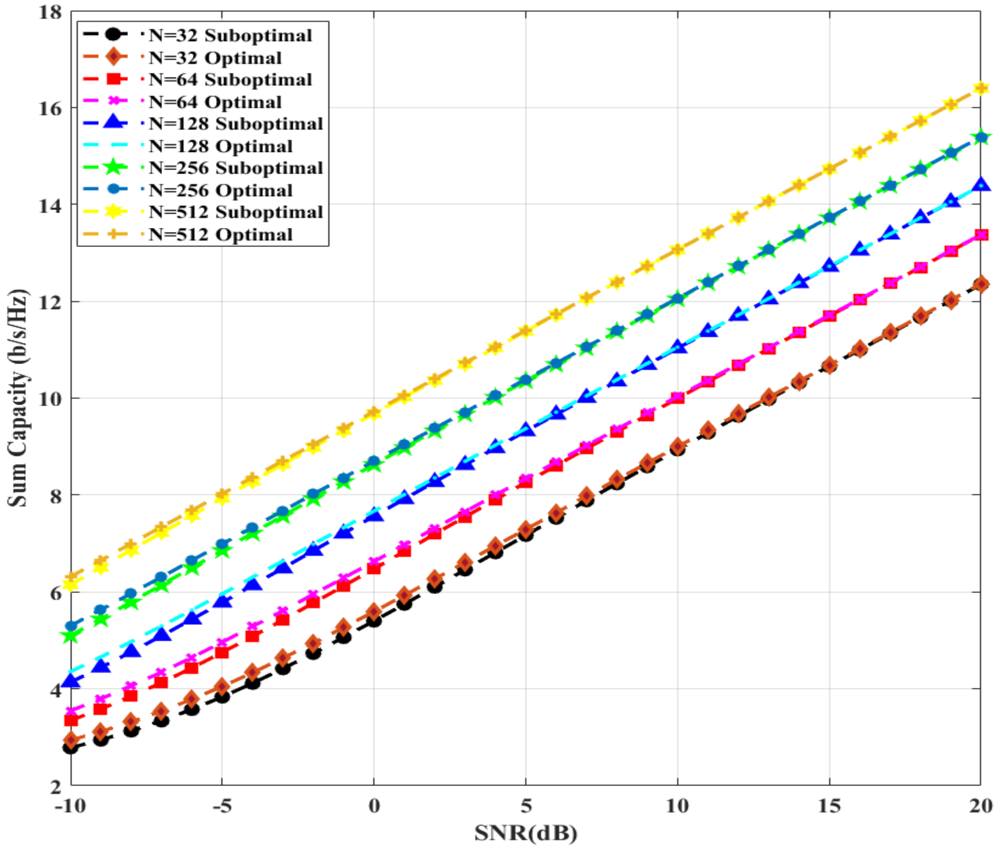

Figure 7. Sum capacity analysis of optimal vs. suboptimal blind RIS-SR-ONOMA for distinct N.

The suboptimal power is the average of α_2^{min} and α_2^{max}. The suboptimal value of α_2 is

$$\alpha_2^{subopt} = \frac{\alpha_2^{min} + \alpha_2^{max}}{2} \tag{48}$$

The suboptimal value of α_1 in RIS-SR-ONOMA is given as

$$\alpha_1^{subopt} = 1 - \alpha_2^{subopt} \tag{49}$$

For all N, optimal power allocation is giving slightly higher capacity than the suboptimal power allocation at low SNR regions. The sum capacity of the system increases with a higher N value. Figures 8–11 examine the performance of blind RIS-AP-ONOMA system. For Figures 8–11, the explanations are the same as those for Figures 3–5 and 7.

Figure 12 compares the sum capacity performance of ONOMA and RIS-based ONOMA systems for 32 passive reflector elements. At 20 dB SNR, the optimal sum capacities observed for blind RIS-AP-ONOMA, blind RIS-SR-ONOMA and ONOMA configurations are 12.3787 b/s/Hz, 12.3557 b/s/Hz and 8.3414 b/s/Hz respectively. With the introduction of RIS in ONOMA, the sum capacity of the system has been increased by ≈33% at SNR of 20 dB for 32 passive reflector elements.

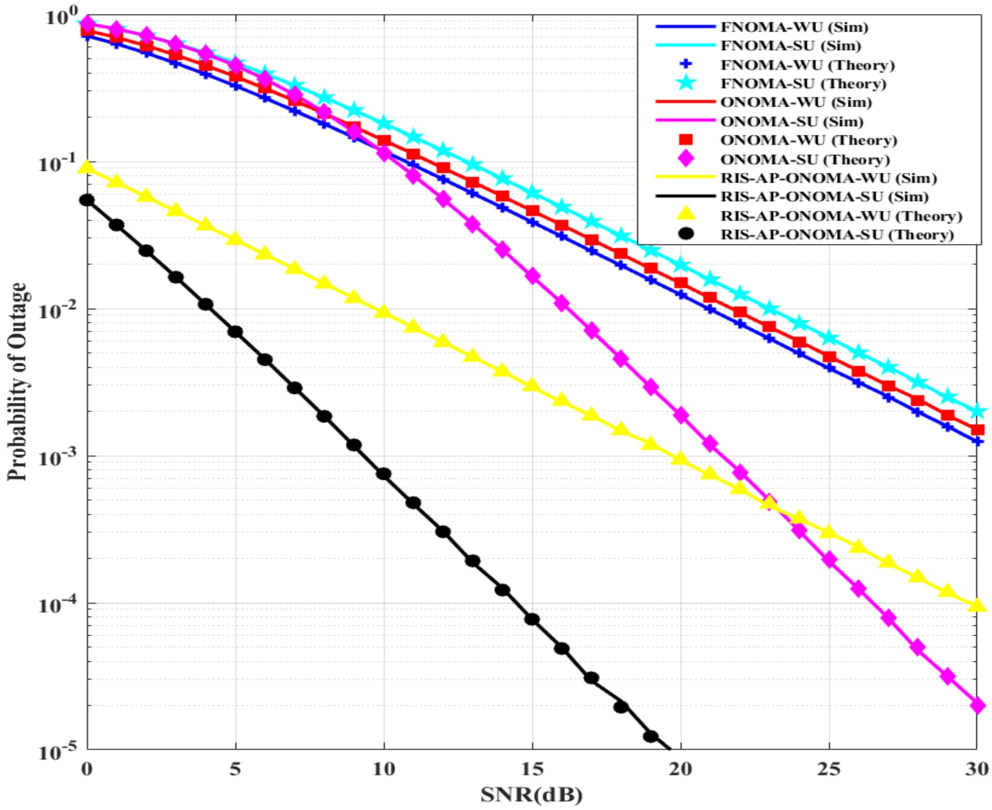

Figure 8. Comparison of probabilities of outage of *WU* and *SU* for FNOMA, ONOMA and blind RIS-AP-ONOMA.

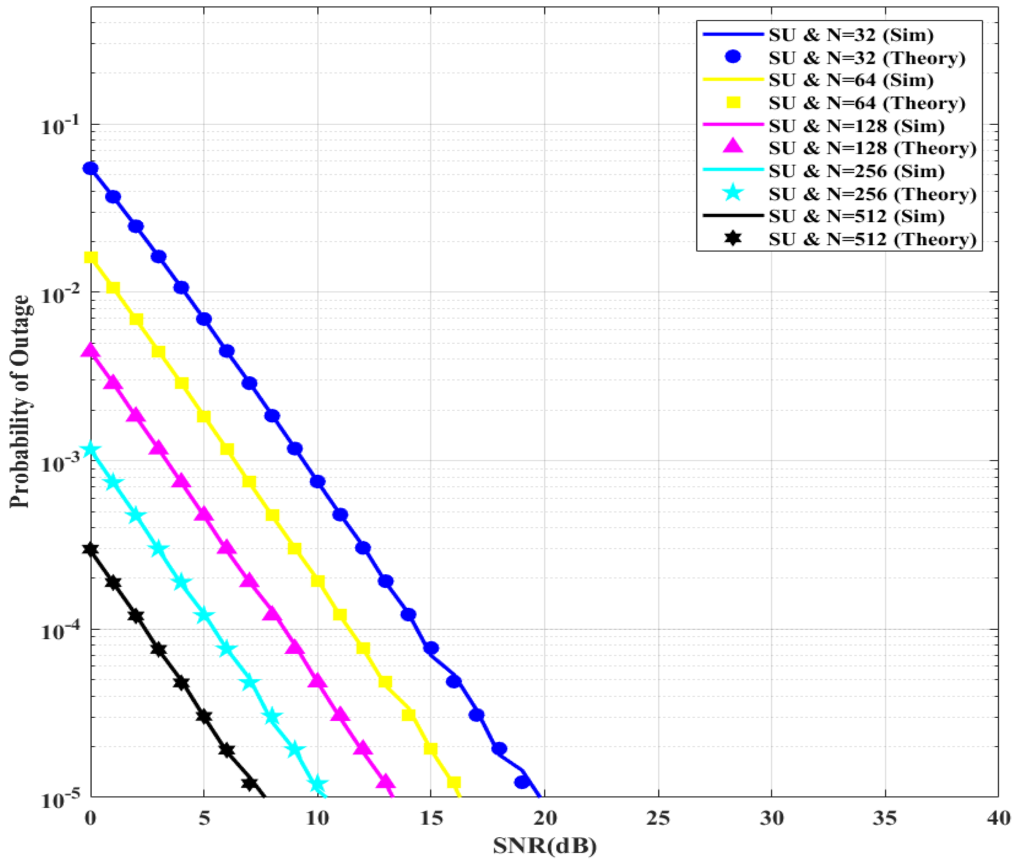

Figure 9. Probability of outage analysis of blind RIS-AP-ONOMA *SU* with distinct *N*.

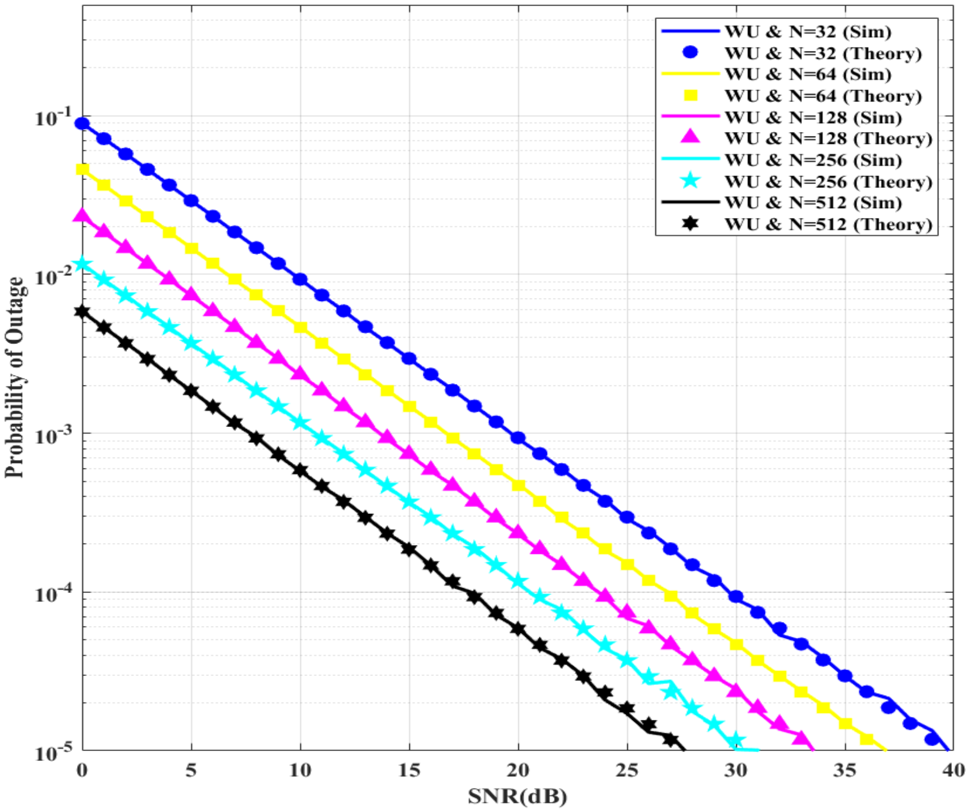

Figure 10. Probability of outage analysis of blind RIS-AP-ONOMA *WU* with distinct *N*.

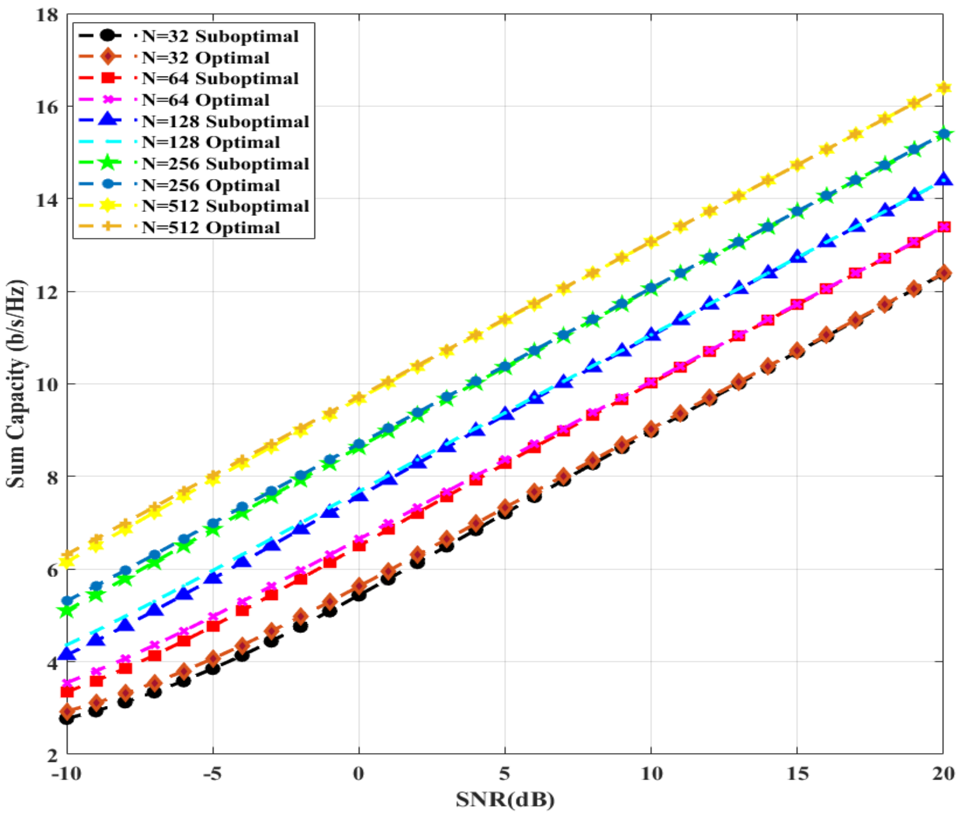

Figure 11. Sum capacity analysis of optimal vs. suboptimal blind RIS-AP-ONOMA for distinct *N*.

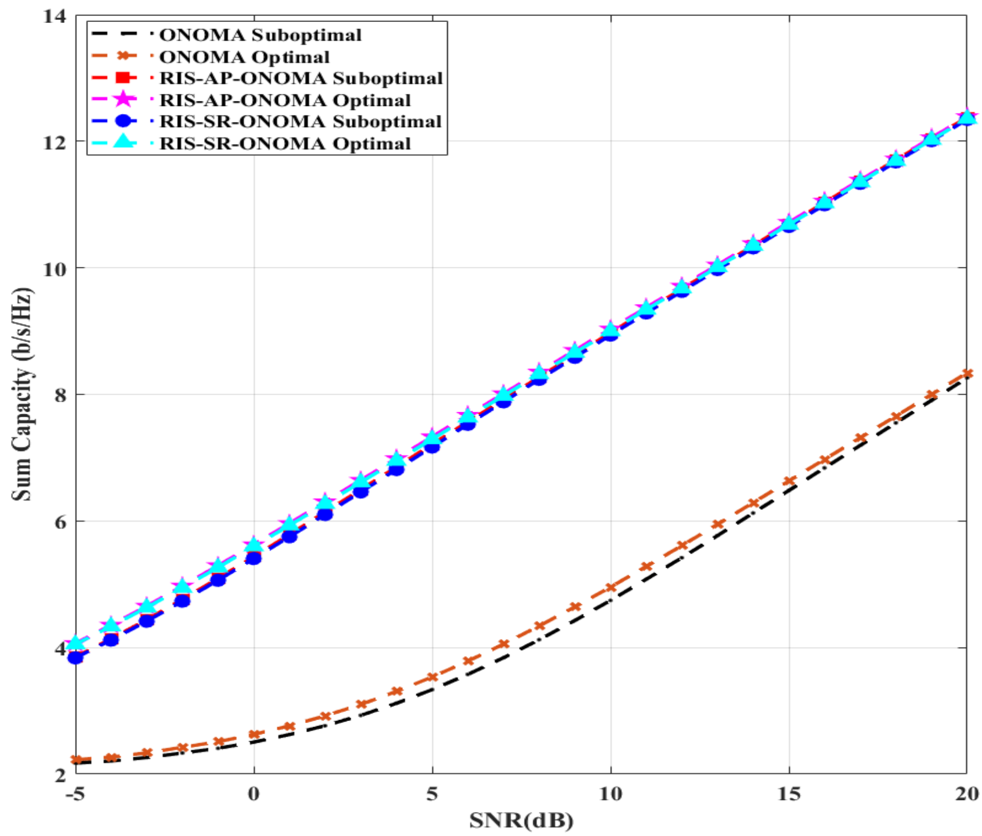

Figure 12. Sum capacity comparison of blind RIS-SR-ONOMA, blind RIS-AP-ONOMA and ONOMA systems.

The throughput expression for RIS-SR-ONOMA is given by [32]

$$\text{TP} = \dot{\text{D}}_{WU}\left(1 - P_{WU}^{o_{SR}}\right) + \dot{\text{D}}_{SU}\left(1 - P_{SU}^{o_{SR}}\right) \tag{50}$$

Figure 13 compares the throughput performance of blind RIS-SR-ONOMA, FNOMA and ONOMA systems. To achieve target throughput of 3/b/s/Hz, FNOMA and ONOMA systems require SNR of ≈30 dB and ≈26 dB, respectively. Since ONOMA system considers channel gains for deciding the decoding order of the users, the SNR required to achieve the target throughput for ONOMA is lower than FNOMA system. Inclusion of RIS decreases SNR requirements. To achieve the same target throughput N = 32, 64, 128, 256 and 512 requires SNRs of ≈11 dB, ≈8 dB, ≈5 dB, ≈2 dB and ≈0 dB respectively. As N increases improvement in performance is observed.

The probability of error curves is developed assuming binary phase shift keying (BPSK) modulation, a path loss exponent of 4, and a bandwidth of 1 MHz. Figure 14 compares the probability of error performance of ONOMA and the RIS-AP-ONOMA *WU* for various N. The probability of error expressions for the *SU* and *WU* of the ONOMA system are developed in [33]. The probability of error of *WU* of ONOMA system is 0.1956 at 5 dB SNR. The probabilities of error of *WU* of RIS-AP-ONOMA system are 0.0277, 0.0146, 0.0075, 0.0038 and 0.0019 for N = 32, 64, 128, 256, and 512 respectively at SNR of 5 dB. Comparing the RIS-AP-ONOMA system to the traditional ONOMA system, a noticeable improvement is seen. Even without phase compensation, the array gain facilitated by the RIS-AP-ONOMA system demonstrates the considerable difference in error probability. The probability of error performance of the proposed system improves with an increase in N.

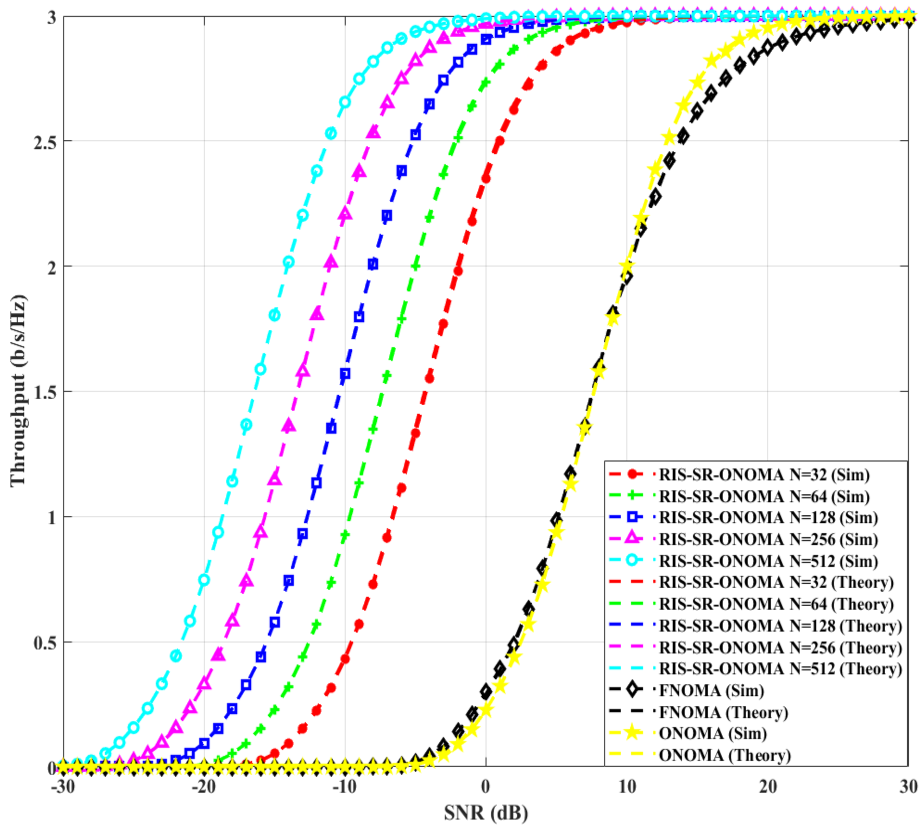

Figure 13. Throughput comparison of blind RIS-SR-ONOMA, FNOMA and ONOMA systems.

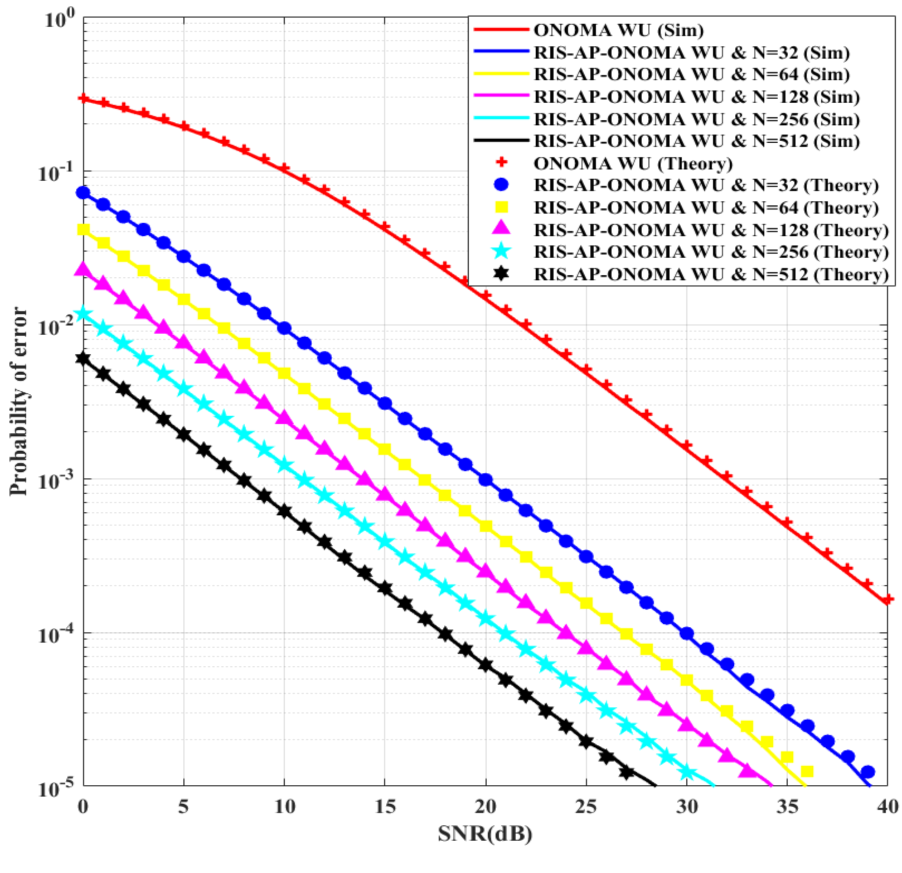

Figure 14. Comparison of probability of error of *WU* for the blind RIS-AP-ONOMA and ONOMA systems.

Similarly, Figure 15 compares the probability of error performance of ONOMA and the RIS-AP-ONOMA *SU* for various *N*. The probability of error of *SU* of ONOMA system is 0.1393 at 5 dB SNR. The probabilities of error observed for *SU* of RIS-AP-ONOMA system are 0.0026, 0.0013, 0.0006, 0.0003, and 0.0001 for *N* = 32, 64, 128, 256, and 512 respectively at SNR of 5 dB. Because of the increased power allocation and higher channel gain, the probability of error for *SU* is much lower than for *WU* in both systems. Additionally, it is noted that the theoretical and simulated probability of error curves closely resemble one another. With an increase in *N*, the proposed system performs better in terms of probability of error.

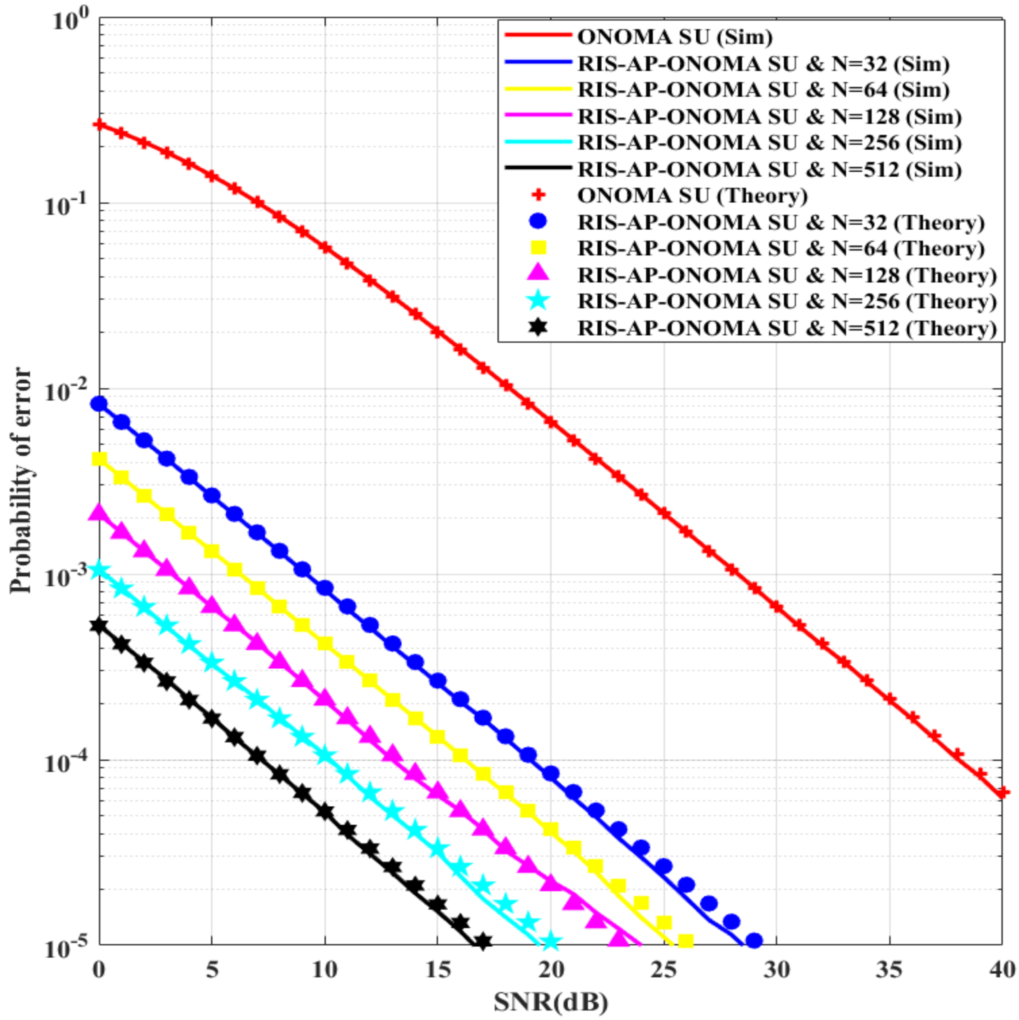

Figure 15. Comparison of probability of error of *SU* for the blind RIS-AP-ONOMA and ONOMA systems.

5. Conclusions

In this work, blind RIS-aided ONOMA system is presented for SR and AP configurations. The closed-form probability of outage expressions is derived for *SU* and *WU* for SR and AP scenarios. Additionally, the optimal power fractions to assign in order to maximize the DL sum capacity are determined. For various values of *N*, the probability of outage, sum capacity, throughput and probability of error performances are investigated. It has been noted that performance for the probability of outage, sum capacity, throughput and probability of error has improved for higher values of *N*. At 20 dB of SNR and for 32 passive reflector elements, the sum capacity of RIS-ONOMA system is increased by ≈33% compared to the ONOMA system. Over the traditional FNOMA and ONOMA systems, RIS-aided ONOMA has a lower outage probability. In future, the same system model could be implemented for UL scenario. For asymmetric DL channel, this approach is tested. This could be studied further for DL symmetric channels, where each user has a similar channel gain. Deep learning or machine learning techniques may be employed for user selection. As a result of the improved performance, we are seeking to generalize the proposed system for multiple users in our future work. The sum capacity can be further enhanced by incorporating user grouping. We also intend to expand the hardware experimentation once the testbeds are commercially available.

Author Contributions: Methodology, H.K.J.; Project administration, V.B.K.; Resources, V.B.K.; Software, H.K.J.; Supervision, V.B.K.; Validation, H.K.J. and V.B.K.; Visualization, H.K.J.; Writing—original draft, H.K.J.; Writing—review & editing, V.B.K. All authors have read and agreed to the published version of the manuscript.

Funding: This work is supported by School of Electronics Engineering, Vellore Institute of Technology, Vellore, Tamil Nadu, India.

Data Availability Statement: The data that support the findings of this paper are available from the corresponding author upon reasonable request.

Conflicts of Interest: The authors declare no conflict of interest.

Appendix A. Proof of PDF of WU

The cumulative distribution function (CDF) of $\widetilde{\beta}_{WU}$ is given by

$$F_{\widetilde{B}_{WU}}\left(\widetilde{\beta}_{WU}\right) = Pr\left(\widetilde{B}_{WU} \leq \widetilde{\beta}_{WU}\right) = 1 - Pr(\widetilde{B}_{WU} > \widetilde{\beta}_{WU}) \tag{A1}$$

From (16), (A1) can be written as

$$F_{\widetilde{B}_{WU}}\left(\widetilde{\beta}_{WU}\right) = 1 - Pr(min(B_1, B_2\ ) > \widetilde{\beta}_{WU} \tag{A2}$$

Since B_1 and B_2 are independent random variables, (A2) is written as

$$F_{\widetilde{B}_{WU}}(\widetilde{\beta}_{WU}) = 1 - Pr\left(B_1 > \widetilde{\beta}_{WU}\ \right) Pr\left(B_2 > \widetilde{\beta}_{WU}\right) \tag{A3}$$

$$Pr(B_1 > \widetilde{\beta}_{WU}) = \int_{\widetilde{\beta}_{WU}}^{\infty} f_{B_1}(\beta_1) d\beta_1 \tag{A4}$$

Substituting (13) in (A4) and simplifying,

$$Pr\left(B_1 > \widetilde{\beta}_{WU}\ \right) = \int_{\widetilde{\beta}_{WU}}^{\infty} \frac{1}{\delta_1^2 N_1} exp\left(\frac{-\widetilde{\beta}_{WU}}{\delta_1^2 N_1}\right) d\beta_1 = exp\left(\frac{-\widetilde{\beta}_{WU}}{\delta_1^2 N_1}\right) \tag{A5}$$

Similarly,

$$Pr\left(B_2 > \widetilde{\beta}_{WU}\ \right) = exp\left(\frac{-\widetilde{\beta}_{WU}}{\delta_2^2 N_2}\right) \tag{A6}$$

Substituting (A5) and (A6) in (A3),

$$F_{\widetilde{B}_{WU}}\left(\widetilde{\beta}_{WU}\right) = 1 - exp\left(\frac{-\widetilde{\beta}_{WU}}{\delta_1^2 N_1}\right) exp\left(\frac{-\widetilde{\beta}_{WU}}{\delta_2^2 N_2}\right) \tag{A7}$$

By differentiating (A7), the PDF of WU is obtained as

$$f_{\widetilde{B}_{WU}}\left(\widetilde{\beta}_{WU}\right) = \frac{d}{d\widetilde{\beta}_{WU}} F_{\widetilde{B}_{WU}}\left(\widetilde{\beta}_{WU}\right) = \left(\frac{1}{\delta_1^2 N_1} + \frac{1}{\delta_2^2 N_2}\right) exp\left(\frac{-\widetilde{\beta}_{WU}}{\delta_1^2 N_1} + \frac{-\widetilde{\beta}_{WU}}{\delta_2^2 N_2}\right) \tag{A8}$$

Substituting (15) in (A8), the expression in (17) is obtained.

Appendix B. Proof of PDF of SU

The CDF of $\widetilde{\beta}_{SU}$ is given by

$$F_{\widetilde{B}_{SU}}\left(\widetilde{\beta}_{SU}\right) = Pr\left(\widetilde{B}_{SU} \leq \widetilde{\beta}_{SU}\right) \tag{A9}$$

From (24), (A9) can be written as

$$F_{\widetilde{B}_{SU}}(\widetilde{\beta}_{SU}) = Pr(max(B_1, B_2\ ) \leq \widetilde{\beta}_{SU}) \tag{A10}$$

Since B_1 and B_2 are independent random variables, (A10) is written as

$$F_{\widetilde{B}_{SU}}(\widetilde{\beta}_{SU}) = \ Pr(B_1 < \widetilde{\beta}_{SU})\ Pr(B_2 < \widetilde{\beta}_{SU}) \tag{A11}$$

$$Pr(B_1 < \widetilde{\beta}_{SU}) = \int_0^{\widetilde{\beta}_{SU}} f_{B_1}(\beta_1) d\beta_1 \tag{A12}$$

Substituting (13) in (A12) and simplifying,

$$Pr(B_1 < \widetilde{\beta}_{SU}) = 1 - exp\left(\frac{-\widetilde{\beta}_{SU}}{\delta_1^2 N_1}\right) \tag{A13}$$

Similarly,

$$Pr(B_2 < \widetilde{\beta}_{SU}) = 1 - exp\left(\frac{-\widetilde{\beta}_{SU}}{\delta_2^2 N_2}\right) \tag{A14}$$

Substituting (A13) and (A14) in (A11),

$$F_{\widetilde{B}_{SU}}\left(\widetilde{\beta}_{SU}\right) = \left(1 - exp\left(\frac{-\widetilde{\beta}_{SU}}{\delta_1^2 N_1}\right)\right)\left(1 - exp\left(\frac{-\widetilde{\beta}_{SU}}{\delta_2^2 N_2}\right)\right) \tag{A15}$$

By differentiating (A15), the PDF of SU is obtained as

$$f_{\widetilde{B}_{SU}}\left(\widetilde{\beta}_{SU}\right) = \frac{d}{d\widetilde{\beta}_{SU}} F_{\widetilde{B}_{SU}}\left(\widetilde{\beta}_{SU}\right) = \frac{1}{\delta_1^2 N_1} exp\left(\frac{-\widetilde{\beta}_{SU}}{\delta_1^2 N_1}\right) + \frac{1}{\delta_2^2 N_2} exp\left(\frac{-\widetilde{\beta}_{SU}}{\delta_2^2 N_2}\right) - \left(\frac{1}{\delta_1^2 N_1} + \frac{1}{\delta_2^2 N_2}\right) exp\left(\frac{-\widetilde{\beta}_{SU}}{\delta_1^2 N_1} + \frac{-\widetilde{\beta}_{SU}}{\delta_2^2 N_2}\right) \tag{A16}$$

Substituting (15) in (A16), the expression in (25) is obtained.

Appendix C. Proof of Feasibility Region

For no outage, user 1 has to satisfy the condition in (36). Substituting (5) in (36) gives

$$log_2\left(1 + \frac{\beta_1 \alpha_1 \varrho_s}{\beta_1 \alpha_2 \varrho_s + 1}\right)\ \geq\ \dot{\mathrm{D}}_{WU} \tag{A17}$$

Taking antilogarithm of both the sides

$$1 + \frac{\beta_1 \alpha_1 \varrho_s}{\beta_1 \alpha_2 \varrho_s + 1} \geq 2^{\dot{\mathrm{D}}_{WU}} \tag{A18}$$

Replacing $\alpha_1 = 1 - \alpha_2$ and simplifying for α_2

$$\alpha_2 \leq \frac{\beta_1 \varrho_s - D_{WU}}{\beta_1 \varrho_s (1 + D_{WU})} \tag{A19}$$

For no outage, user 2 has to satisfy the condition in (37). By following the same procedure like user 1, the feasibility region for user 2 is estimated which is given by

$$\alpha_2 \geq\ \frac{D_{SU}}{\beta_2 \varrho_s} \tag{A20}$$

By combining (A19) and (A20), the condition in (39) is obtained.

References

1. Giordani, M.; Polese, M.; Mezzavilla, M.; Rangan, S.; Zorzi, M. Toward 6G Networks: Use Cases and Technologies. *IEEE Commun. Mag.* **2020**, *58*, 55–61. [CrossRef]
2. Tariq, F.; Khandaker, M.R.; Wong, K.K.; Imran, M.A.; Bennis, M.; Debbah, M. A speculative study on 6G. *IEEE Wirel. Commun.* **2020**, *27*, 118–125. [CrossRef]
3. Dang, S.; Amin, O.; Shihada, B.; Alouini, M.S. What should 6G be? *Nat. Electron.* **2020**, *3*, 20–29. [CrossRef]
4. Akhtar, M.W.; Hassan, S.A.; Ghaffar, R.; Jung, H.; Garg, S.; Hossain, M.S. The shift to 6G communications: Vision and requirements. *Human-Centric Comput. Inf. Sci.* **2020**, *10*, 53. [CrossRef]
5. Vaezi, M.; Baduge, G.A.A.; Liu, Y.; Arafa, A.; Fang, F.; Ding, Z. Interplay between NOMA and other emerging technologies: A survey. *IEEE Trans. Cogn. Commun. Netw.* **2019**, *5*, 900–919. [CrossRef]
6. Imoize, A.; Adedeji, O.; Tandiya, N.; Shetty, S. 6G Enabled Smart Infrastructure for Sustainable Society: Opportunities, Challenges, and Research Roadmap. *Sensors* **2021**, *21*, 1709. [CrossRef]
7. Liu, Y.; Zhang, S.; Mu, X.; Ding, Z.; Schober, R.; Al-Dhahir, N.; Hossain, E.; Shen, X. Evolution of NOMA Toward Next Generation Multiple Access (NGMA) for 6G. *IEEE J. Sel. Areas Commun.* **2022**, *40*, 1037–1071. [CrossRef]
8. Badarudeena, S. Performance of antenna selection schemes for massive multiple-input multiple-output systems under Non-orthogonal multiple access cooperative communication. *Indian J. Radio Space Phys. (IJRSP)* **2022**, *50*, 46–50.
9. Ding, Y.; Kim, K.J.; Koike-Akino, T.; Pajovic, M.; Wang, P.; Orlik, P. Spatial scattering modula-tion for uplink millimeter-wave systems. *IEEE Commun. Lett.* **2017**, *21*, 1493–1496. [CrossRef]
10. Ding, Y.; Fusco, V.; Shitvov, A.; Xiao, Y.; Li, H. Beam Index Modulation Wireless Communication with Analog Beamforming. *IEEE Trans. Veh. Technol.* **2018**, *67*, 6340–6354. [CrossRef]
11. Basar, E. Transmission through Large Intelligent Surfaces: A New Frontier in Wireless Communications. In Proceedings of the 2019 European Conference on Networks and Communications (EuCNC), Valencia, Spain, 18–21 June 2019; pp. 112–117. [CrossRef]
12. Liaskos, C.; Nie, S.; Tsioliaridou, A.; Pitsillides, A.; Ioannidis, S.; Akyildiz, I. A New Wireless Communication Paradigm through Software-Controlled Metasurfaces. *IEEE Commun. Mag.* **2018**, *56*, 162–169. [CrossRef]
13. Wang, J.; Tang, W.; Han, Y.; Jin, S.; Li, X.; Wen, C.-K.; Cheng, Q.; Cui, T.J. Interplay Between RIS and AI in Wireless Communications: Fundamentals, Architectures, Applications, and Open Research Problems. *IEEE J. Sel. Areas Commun.* **2021**, *39*, 2271–2288. [CrossRef]
14. Zhao, J. A survey of intelligent reflecting surfaces (IRSs): Towards 6G wireless communication networks. *arXiv* **2019**, arXiv:1907.04789.
15. Chen, A.; Chen, Y.; Wang, Z. Reconfigurable Intelligent Surface Deployment for Blind Zone Im-provement in MmWave Wireless Networks. *IEEE Commun. Lett.* **2022**, *26*, 1423–1427. [CrossRef]
16. Trichopoulos, G.C.; Theofanopoulos, P.; Kashyap, B.; Shekhawat, A.; Modi, A.; Osman, T.; Kumar, S.; Sengar, A.; Chang, A.; Alkhateeb, A. Design and Evaluation of Reconfigurable Intelligent Surfaces in Real-World Environment. *IEEE Open J. Commun. Soc.* **2022**, *3*, 462–474. [CrossRef]
17. Jian, M.; Alexandropoulos, G.C.; Basar, E.; Huang, C.; Liu, R.; Liu, Y.; Yuen, C. Reconfigurable intelligent surfaces for wireless communications: Overview of hardware designs, channel models, and estimation techniques. *Intell. Converg. Netw.* **2022**, *3*, 1–32. [CrossRef]
18. Miridakis, N.I.; Tsiftsis, T.A.; Yang, G.; Karkazis, P.A.; Leligou, H.C. Semi-Blind Multiuser Detection under the Presence of Reconfigurable Intelligent Surfaces. *IEEE Wireless Commun. Lett.* **2021**, *11*, 106–110. [CrossRef]
19. Islam, S.M.; Zeng, M.; Dobre, O.A.; Kwak, K.S. Non-orthogonal multiple access (NOMA): How it meets 5G and beyond. *arXiv* **2019**, arXiv:1907.10001.
20. Huang, Y.; Zhang, C.; Wang, J.; Jing, Y.; Yang, L.; You, X. Signal Processing for MIMO-NOMA: Present and Future Challenges. *IEEE Wirel. Commun.* **2018**, *25*, 32–38. [CrossRef]
21. Thirumavalavan, V.C.; Jayaraman, T.S. BER analysis of reconfigurable intelligent surface assisted downlink power domain NOMA system. In Proceedings of the 2020 International Conference on COMmunication Systems & NETworkS (COMSNETS), Bengaluru, India, 7–11 January 2020; pp. 519–522.
22. Zhang, C.; Yi, W.; Liu, Y.; Qin, Z.; Chai, K.K. Downlink Analysis for Reconfigurable Intelligent Surfaces Aided NOMA Networks. In Proceedings of the GLOBECOM 2020—2020 IEEE Global Communications Conference, Taipei, Taiwan, 7–11 December 2020; pp. 1–6. [CrossRef]
23. Al-Nahhal, I.; Dobre, O.A.; Basar, E. Reconfigurable Intelligent Surface-Assisted Uplink Sparse Code Multiple Access. *IEEE Commun. Lett.* **2021**, *25*, 2058–2062. [CrossRef]
24. Li, G.; Liu, H.; Huang, G.; Li, X.; Raj, B.; Kara, F. Effective capacity analysis of reconfigurable intelligent surfaces aided NOMA network. *EURASIP J. Wirel. Commun. Netw.* **2021**, *2021*, 198. [CrossRef]
25. Tahir, B.; Schwarz, S.; Rupp, M. RIS-Assisted Code-Domain MIMO-NOMA. In Proceedings of the 2021 29th European Signal Processing Conference (EUSIPCO), Dublin, Ireland, 23–27 August 2021; pp. 821–825.

26. Zhang, Z.; Zhang, C.; Jiang, C.; Jia, F.; Ge, J.; Gong, F. Improving Physical Layer Security for Reconfigurable Intelligent Surface Aided NOMA 6G Networks. *IEEE Trans. Veh. Technol.* **2021**, *70*, 4451–4463. [CrossRef]
27. Basar, E.; Di Renzo, M.; De Rosny, J.; Debbah, M.; Alouini, M.-S.; Zhang, R. Wireless Communications through Reconfigurable Intelligent Surfaces. *IEEE Access* **2019**, *7*, 116753–116773. [CrossRef]
28. Agarwal, A.; Chaurasiya, R.; Rai, S.; Jagannatham, A.K. Outage Probability Analysis for NOMA Downlink and Uplink Communication Systems with Generalized Fading Channels. *IEEE Access* **2020**, *8*, 220461–220481. [CrossRef]
29. Salo, J.; El-Sallabi, H.; Vainikainen, P. The Distribution of the Product of Independent Rayleigh Random Variables. *IEEE Trans. Antennas Propag.* **2006**, *54*, 639–643. [CrossRef]
30. Nguyen, H.-N.; Le, C.-B.; Nguyen, N.-T.; Do, D.-T. Study on outage performance gap of two destinations on CR-NOMA network. *TELKOMNIKA (Telecommun. Comput. Electron. Control.)* **2020**, *18*, 191–198. [CrossRef]
31. Do, D.-T.; Le, C.-B. Exploiting performance gap among two users in reconfigurable intelligent surfaces-aided wireless systems. *TELKOMNIKA (Telecommun. Comput. Electron. Control.)* **2022**, *20*, 1–8. [CrossRef]
32. Hemanth, A.; Umamaheswari, K.; Pogaku, A.C.; Do, D.-T.; Lee, B.M. Outage performance analysis of reconfigurable intelligent surfaces-aided NOMA under presence of hardware impairment. *IEEE Access* **2020**, *8*, 212156–212165. [CrossRef]
33. Kara, F.; Kaya, H. BER performances of downlink and uplink NOMA in the presence of SIC errors over fading channels. *IET Commun.* **2018**, *12*, 1834–1844. [CrossRef]